CO Oxidation on Pt: Model Discrimination Using Experimental Bifurcation Behavior

An experimental determination of the steady state behavior for the supported platinum catalyzed oxidation of carbon monoxide in a recycle reactor was performed. Steady state multiplicity was observed. The effects of the size of catalyst charge, feed flow rate, feed composition, and reactor temperature on the location of the boundaries of the steady state multiplicity region were determined. The sensitivity of these bifurcation points to variations in reactor parameters was used to discriminate among five reaction mechanisms. Only an elementary step model incorporating carbon monoxide self-exclusion from the catalyst surface could quantitatively describe all observed steady state data. An explicit rate function based on this model is presented.

W. R. C. Graham and D. T. Lynch
Department of Chemical Engineering
University of Alberta
Edmonton, Alberta, Canada T6G 2G6

Introduction

The occurrence of multiple steady states in the operation of chemical reactors has been recognized for almost seventy years (Liljenroth, 1918). While the operation of an industrial reactor in a multiple steady state region is usually avoided, multiplicity behavior can provide valuable insight into reaction mechanisms. The causes of steady state multiplicity include autothermicity (van Heerden, 1953), reaction rate inhibition due to competitive adsorption (Matsuura and Kato, 1967; Beusch et al., 1972), diffusion-reaction interactions (Hegedus et al., 1977), and autocatalysis (Gray and Scott, 1983).

Reaction rate multiplicity has often been observed for the oxidation of carbon monoxide over noble metal catalysts. The catalyst most often studied has been platinum. For isothermal reactor operation, this reaction displays conversions of CO near 100% at low CO concentrations, and low conversions (less than 10%) at high CO concentrations. At intermediate CO concentrations both high- and low-conversion steady states can occur. This behavior has been observed in continuous stirred-tank reactors (CSTR) (Cutlip, 1979) and tubular reactors (Hegedus et al., 1977) using Pt wires, gauze, and foils, and supported platinum catalysts. Although there are many suggested explanations for CO oxidation multiplicity behavior, there is a dearth of detailed studies of the effect on multiplicity behavior of reactor parameters such as temperature, feed flow rate, feed composition, and size of catalyst charge. Cutlip (1979) and Graham and Lynch (1985) examined the effect of temperature and composition on the region of multiple steady states. Graham and Lynch modeled these effects using an elementary step Langmuir-Hinshelwood (LH) mechanism. Oh et al. (1979) investigated the effect of catalyst particle size on multiplicity behavior. They showed that hysteresis was eliminated when catalyst particle size became sufficiently small. Chakrabarty et al. (1984) examined the effect of diluent gases on the region of multiplicity and concluded that the reaction-sorption interference explanation cannot be overlooked. Herskowitz and Kenney (1983) examined the effects of temperature and feed composition on multiplicity behavior. They used three Langmuir-Hinshelwood Hougen-Watson (LHHW) models to describe the reaction system, and found that two of them could accurately predict the transition from the low-conversion steady state rate branch to the high-conversion rate branch. However, no comparisons were made concerning the high to low conversion bifurcation point. Mukesh et al. (1984) have used an elementary step Langmuir-Hinshelwood mechanism incorporating CO surface island formation to describe the low-conversion branch of the steady state rate curve. This model was also able to describe the dynamic response of a CSTR to step changes in feed composition.

Heinemann et al. (1979) suggested that bifurcation theory could be used to identify unknown parameters in physical systems. Conrad and Treguer-Seguda (1984) have investigated how the knowledge of a bifurcation point can lead to parameter estimates. They presented an algorithm for estimating parameters and demonstrated its use through examples concerned with thermal ignition and enzymatic diffusion-reaction. As demonstrated by Herskowitz and Kenney (1983), a knowledge of the bifurcation behavior of a physical system can also aid in discrim-

Correspondence concerning this paper should be addressed to D. T. Lynch.

ination among rival models. Aluko and Chang (1986) utilized the effect of temperature and composition on the bifurcation behavior of the CO oxidation reaction in order to obtain rate parameter estimates for a kinetic model based on oxidation and reduction of the surface platinum.

In this study, it will be shown that a knowledge of the effect of operating parameters on the multiplicity behavior of a reaction can be used to discriminate among rival kinetic models. This will be done by systematically examining the effects of reactor temperature, feed flow rate, feed composition, and size of catalyst charge on the steady state multiplicity behavior of the carbon monoxide oxidation reaction on a supported platinum catalyst in a recycle reactor. In particular, the sensitivity of the location of the bifurcation points to the reactor operating parameters will be determined. The data will be used to discriminate among five steady state kinetic models that have been proposed for this reaction. All of the models examined are of the elementary step Langmuir-Hinshelwood form. It will be shown that the classical LH mechanism is incapable of quantitatively describing both the reaction rates and the location of the bifurcation points. However, a model that incorporates CO self-exclusion from the catalyst surface is able to quantitatively describe all observed steady state data.

Experimental Equipment and Materials

The recycle reactor system and chemical analysis equipment used in this study have been previously described (Lynch and Wanke, 1984). However, from improved measurements of the equipment, the total reactor volume was determined to be 245 cm^3 with a recycle flow rate of approximately 500 cm^3/s. The reactor pressure was always maintained at 0.1 MPa, and the temperatures used in this study were 70, 90, and 110°C.

The feed composition and flow rate were controlled by three Matheson model 8250 series flow controllers that were interfaced to a HP minicomputer. The computer was used to manipulate the set points of the three flow controllers to obtain the desired feed composition and flow rate. Flow rates between 6 and 3,000 cm^3/min (SCCM) could be accurately set. Standard conditions of 101 kPa and 21°C were used for all flow measurements. All gases used in this study were either Matheson ultra-high-purity grade, or equivalent, or were specialty mixtures of O_2/N_2 and CO/N_2 prepared by Matheson. Feed compositions were in the ranges 0–1.1% O_2 and 0–2% CO, with nitrogen for the balance of the feed.

The catalyst used in this study was purchased from Aldrich and contained 0.5 wt. % platinum supported on γ-Al_2O_3 with a Pt dispersion of approximately 0.5 to 0.6 calculated from hydrogen adsorption measurements. The catalyst support had a BET surface area of 108 m^2/g and an average pore radius of 3 nm. The cylindrical pellets were approximately 3 mm by 3 mm in size, with the Pt deposited in a thin layer on the exterior portion of the pellets. The size of the reactor limited the maximum catalyst charge to 50 g. For catalyst charges of less than 50 g, the bed was diluted with inert glass spheres so that the bed volume was approximately constant at 35 cm^3 for all catalyst charges. Catalyst charges of 4.95, 14.6, and 43.6 g were used in this study.

Experimental Steady State Behavior

The experimental work was concerned with determining the effects of the reactor temperature, feed flow rate, and size of catalyst charge on the rate and multiplicity behavior. Particular attention was paid to determining the feed compositions at which bifurcations occurred (both high to low conversion transitions and low to high conversion transitions). In the following, the term "location of a bifurcation point" refers to the fraction CO in the reactor feed, F_{CO}, at which a bifurcation occurs. The bifurcation point locations depend in a very nonlinear fashion on the reactor operating parameters (temperature, flow rate, etc.). Thus, they are very useful for model discrimination and parameter estimation.

In this study, the exact values of the bifurcation points were not determined, rather their values were bracketed by the following procedure. The total feed flow rate, reactor temperature, and oxygen feed composition were set at desired levels. The CO feed concentration was set at about twice the oxygen concentration. The near-stoichiometric mixture invariably led to a low-conversion steady state. When steady state was achieved the CO concentration was decreased slightly. In this manner the reaction rate curve was determined for decreasing CO feed concentration. The rate curve was also determined for increasing CO feed concentration. The adsorption/desorption of CO_2 from the catalytically inert Al_2O_3 support made the quantitative determination of the low-conversion steady states difficult. Operating times of greater than 24 h were on occasion required to achieve a reproducible low-conversion steady state.

In Figure 1 the results of this procedure are summarized for 1.0% O_2, 14.6 g of catalyst, a feed flow rate of 300 cm^3/min, and a reactor temperature of 90°C. At high CO feed concentrations the reactor operated at a low-conversion steady state, shown by solid circles in Figure 1. Decreasing the CO in the feed caused the conversion to increase gradually from 5% at 1.8% CO to 55% at 0.25% CO. Further decreases in feed CO below 0.25% caused the rate to increase to a steady state with a conversion of 100%, represented by open circles in Figure 1. The reactor remained in a high-conversion steady state when the CO feed concentration was decreased further. Subsequent increases in the percentage CO in the feed resulted in the reactor operating at a high-conversion steady state. The reactor remained in a high-conversion steady state until 1.25% CO in the feed was reached. Increasing the CO in the feed beyond 1.25% caused the reaction rate to drop to the low-conversion steady state. Thus, as shown in Fig-

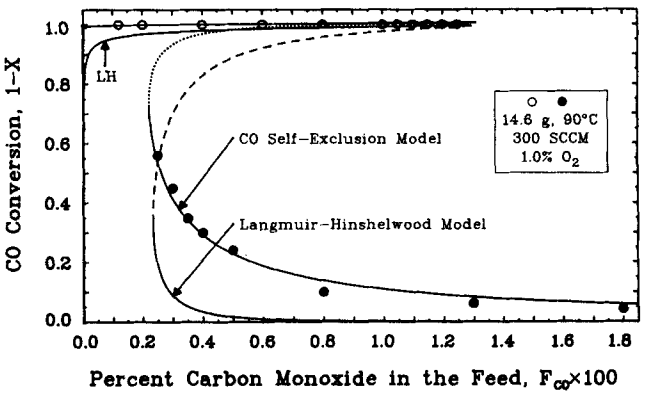

Figure 1. Steady state CO conversion multiplicity.
— Stable steady state
----- Unstable steady state
..... Unstable steady state

ure 1, this reaction displays multiplicity behavior over an intermediate range of values of the %CO in the feed (constant $\%O_2$). In the multiplicity region, the starting conditions determine whether the reactor will operate at a low-conversion or at a high-conversion steady state.

The multiplicity behavior was also determined for O_2 concentrations other than that used in Figure 1, and these results are summarized in Figure 2 where the transition points are shown as functions of the reactor feed composition. The pairing of a half-filled symbol with an empty symbol brackets the low-conversion to high-conversion transition conditions, while the pairing of a half-filled symbol with a filled symbol brackets the high-conversion to low-conversion transition conditions. Thus, the leftmost region in Figure 2 is the high-conversion region, while the rightmost part is the low-conversion region. The cusp-shaped region delimits the conditions under which multiple steady states occur.

Additional experimental data on the variation of the steady state bifurcation boundaries have been collected to enable discrimination among kinetic models. Shown in Figure 3 are the effects of bulk temperature on the bifurcation boundaries. The boundaries at 90°C from Figure 2 are reproduced in Figure 3 (circles) to facilitate comparison between the figures. From Figure 3 it is seen that both the lower and upper experimental bifurcation boundaries shifted to progressively higher CO concentrations as the temperature was increased from 70 to 110°C. An Arrhenius plot of the bifurcation points is shown in Figure 4. The fraction of CO in the feed at the bifurcation points, normalized with respect to that for the bifurcation points at 90°C, is plotted vs. inverse temperature. The low to high conversion bifurcation points have an apparent activation energy of E/R = 5,130 K. The high to low conversion bifurcation points have a slope corresponding to E/R = 2,200 K in the low-temperature region. At higher temperatures the high to low conversion bifurcation points approach stoichiometric mixtures, and the activation energy decreases so that the average value over the entire temperature region is E/R = 1,930 K as shown in Figure 4.

The steady state behavior of the reactor was also examined for flow rates of 100, 300, and 900 cm³/min. Figure 5 shows the effect of flow rate on the bifurcation behavior of the system. As the flow rate was increased, both the upper and lower bifurcation boundaries moved to lower CO concentrations. The relationship between the bifurcation point locations and flow rate is shown in Figure 6. All of the low to high conversion bifurcation points varied inversely with the 0.66 power of flow rate ($\propto Q^{-0.66}$). However, this was not the case with the high to low conversion bifurcation points. At low flow rates, these bifurcation points occurred at conditions corresponding to near-stoichiometric mixtures, and the locations of the bifurcation points were nearly independent of the flow rate. For large flow rates, the high to low conversion bifurcation points depended inversely on flow rate to the 0.72 power. Thus, as shown in Figure 6, over the range of flow rates examined the high to low conversion bifurcation points varied according to $Q^{-0.43}$ on average.

The experimental effects of temperature and feed flow rate on the bifurcation point locations will be used in the following as the basis for discrimination among several models for this reaction.

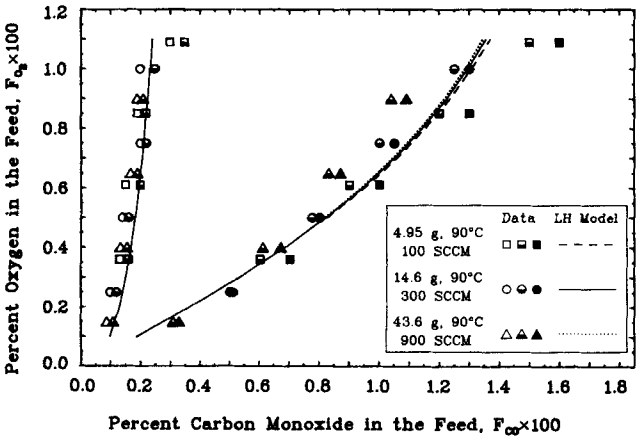

Figure 2. Multiplicity boundaries for three catalyst charges.

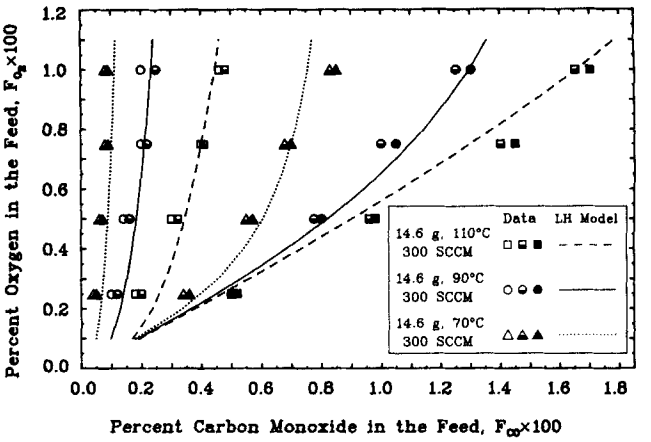

Figure 3. Effect of temperature on multiplicity boundaries.

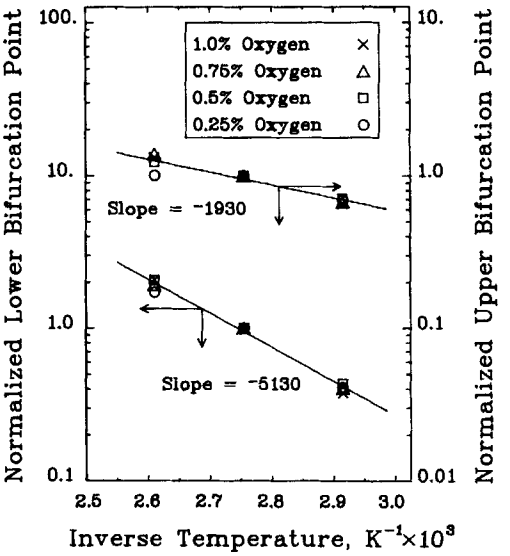

Figure 4. Dependence of bifurcation points on temperature.

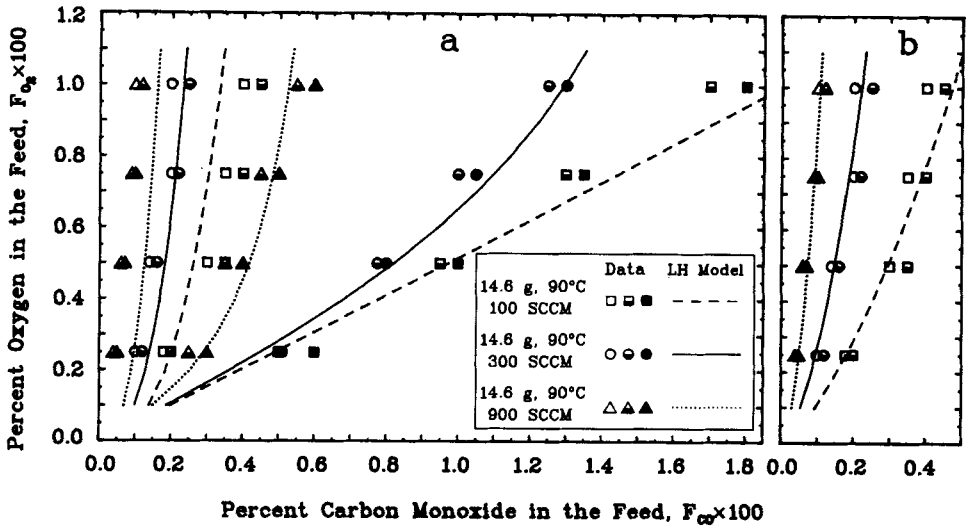

Figure 5. Effect of flow rate on multiplicity boundaries.
a. Langmuir-Hinshelwood model
b. CO self-exclusion model

Mathematical Models

It is generally accepted that at the temperatures studied, the catalytic oxidation of CO on platinum occurs via the following steps:

$$CO(g) + M \underset{k_{-1}}{\overset{k_1}{\rightleftharpoons}} CO - M \tag{1}$$

$$O_2(g) + 2M \xrightarrow{k_2} 2O - M \tag{2}$$

$$CO - M + O - M \xrightarrow{k_3} CO_2(g) + 2M \tag{3}$$

where M is a metal (platinum) surface site.

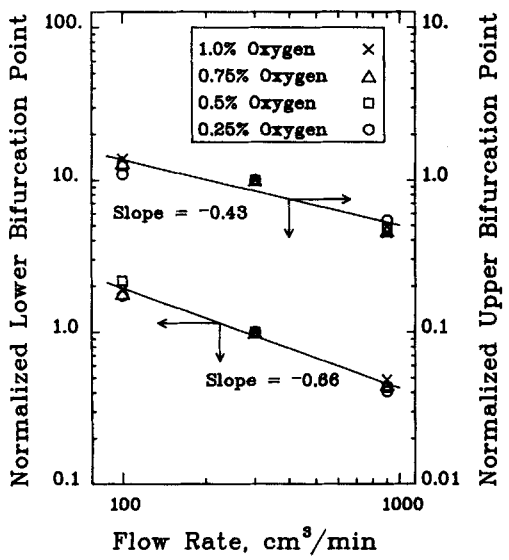

Figure 6. Dependence of bifurcation points on flow rate.

CO adsorbs reversibly on a single platinum surface site. Oxygen adsorbs dissociatively and irreversibly. The two surface species undergo a bimolecular reaction forming CO_2, which immediately desorbs, freeing two surface metal sites.

The reactor used in this study can be modeled as a CSTR due to the high recycle ratios that were employed. In the absence of inter- and intrapellet heat and mass transfer limitations, mass balances on the various gas and surface phase species produce the following five ordinary differential equations (see the notation for symbol definitions):

$$\frac{dX}{d\tau} = X_o - Q_n X - R_1 \tag{4}$$

$$\frac{dY}{d\tau} = Y_o - Q_n Y - R_2 \tag{5}$$

$$\frac{dZ}{d\tau} = Z_o - Q_n Z - R_3 \tag{6}$$

$$\frac{d\theta_{CO}}{d\tau} = \alpha_m \{R_1 - R_3\} \tag{7}$$

$$\frac{d\theta_O}{d\tau} = \alpha_m \left\{ \frac{2F_{O_2}}{F_{CO}} R_2 - R_3 \right\} \tag{8}$$

where

$$Q_n = 1 - F_{CO} R_1 - F_{O_2} R_2 + F_{CO} R_3 \tag{9}$$

The terms R_1, R_2, and R_3 refer to the net rates of steps 1, 2, and 3, respectively. The forms of the R_i terms depend on the details

of the various mechanisms. Equations 4 to 8 have been written in differential rather than algebraic form so that they may readily be used in conjunction with studies concerned with reaction dynamics. However, since steady state behavior is the focus of the present study, these equations were normally used in algebraic form by setting the derivatives equal to zero. For steady state operation the normalized CO and O_2 feed concentrations, X_o and Y_o, are equal to unity. The steady state models examined in detail herein include an elementary step LH model and a CO self-exclusion model. Three other models were examined in this study and are presented in detail in the Supplementary Material. These are:

1. Surface oxidation-reduction model
2. CO surface island model
3. Modified CO surface island model with oxygen adsorption based on the island-free area

Langmuir-Hinshelwood model

The first mechanism used to describe the reactor behavior was a classical elementary step Langmuir-Hinshelwood type model. Herskowitz and Kenney (1983) showed that a classical LH model, with the surface reaction controlling the overall reaction rate and with both CO and O_2 at equilibrium, was unable to predict most of their experimental bifurcation points. Goodman et al. (1982), however, have used an elementary step LH model to describe the response of the CO-O_2-Pt system to step changes in reactant concentrations. They did not discuss the ability of the model to predict the bifurcation behavior of the system. For the LH model the reaction rates for steps 1 to 3 are as follows:

$$R_1 = K_1 X(1 - \theta_{CO} - \theta_O) - K_{-1}\theta_{CO} \tag{10}$$

$$R_2 = K_2 Y(1 - \theta_{CO} - \theta_O)^2 \tag{11}$$

$$R_3 = K_3 \theta_{CO}\theta_O \tag{12}$$

At steady state the time derivatives in Eqs. 4 to 8 are set equal to zero. These algebraic equations were solved using a differential arclength homotopy-continuation method (Kubicek, 1976). A finite-difference approximation of the Jacobian matrix was used as a check of the stability of the steady state solution. Kinetic parameters were selected to minimize the sum of the squared errors in the predicted locations of the bifurcation points. As a further check of model accuracy, the sum of squared errors in the predicted reaction rates was calculated.

Examination of the definitions of the dimensionless rate constants of the LH model (see Notation) shows that wherever the metal surface area, a_m, appears it is divided by the volumetric feed flow rate, Q_o. This suggests a first test of the proposed model. If the ratio of the mass of catalyst to the volumetric flow rate is constant, then a_m/Q_o is constant, and thus identical values of the dimensionless rate constants are obtained for each catalyst charge. The data in Figure 2 are for catalyst charges of 4.95, 14.6, and 43.6 g. The multiplicity bounds are approximately the same in each case because the total volumetric flow rates, 100, 300, and 900 cm^3/min, respectively, were adjusted so that the ratio of the mass of catalyst to volumetric flow rate was approximately constant for each charge. The slight differences between the three sets of data are due to the small variations in this ratio. The fact that experimentally the multiplicity boundaries are almost the same for all three sets of data is a first, and very important, point of agreement with the proposed model.

The second test for the model is to determine if it can describe the experimentally observed multiplicity behavior shown in Figures 2, 3, and 5. The predicted multiplicity boundaries of the elementary step LH model for a particular set of parameter values, given in Table 1, are shown by the curves in Figures 2, 3, and 5, where in Figure 2 the different curves are for the slightly different values of the a_m/Q_o ratio that were used experimentally. The parameter values were arrived at by minimizing the sum of the squares of the errors between the predicted and the experimental locations of the 40 bifurcation points presented in Figures 3 and 5.

In the process of estimating the parameters, it was found that if only the 24 bifurcation points shown in Figure 3 were used, then many sets of parameters (with quite different values) could all lead to the quantitative prediction of the 24 bifurcation points. This is partially due to the effects of the values of E_{-1} and E_3 being essentially decoupled. The variation of the location of the boundaries for the transition from low to high conversions (leftmost boundaries in Figures 2 and 3) is mainly affected by the value of E_{-1}, while the value of E_3 is the most important parameter in determining the manner in which the high to low conversion boundaries shift under the influence of temperature. Reasonably precise parameter estimates only occurred when all 40 bifurcation points were used.

From Figures 2, 3, and 5 it is seen that excellent prediction of the bifurcation point locations occurs, with the one exception that the LH model significantly underpredicts the effect of flow rate on the location of the low to high conversion bifurcation curve (leftmost curves in Figure 5). Experimentally, the bifurcation points varied as $Q^{-0.66}$ while the LH model predicts they will vary as $Q^{-0.33}$. The inability of the LH model to predict the effect of flow rate on the location of the low to high conversion bifurcation points can be understood by examining a simplified form of the model.

At steady state, the rates of the various reaction steps are identical, thus, from Eqs. 4 to 12:

$$1 - Q_n X = R_1 = R_3 = \frac{2F_{O_2}}{F_{CO}} R_2 = \frac{2F_{O_2}}{F_{CO}} K_2 Y(1 - \theta_{CO} - \theta_O)^2 \tag{13}$$

The CO adsorption and desorption steps in Eq. 1 proceed very rapidly. Thus, for the situation of low conversions, the CO adsorption/desorption will be essentially at equilibrium. Thus, from Eq. 10, the fraction of empty sites will approximately be given by:

$$(1 - \theta_{CO} - \theta_O) = \frac{K_{-1}\theta_{CO}}{K_1 X} \tag{14}$$

However, in order to obtain agreement between the experimental and predicted bifurcation points it was necessary for K_1 to be much greater than K_{-1}, which results in θ_{CO} being approximately unity. Also, since oxygen is in excess, and the CO conver-

Table 1. Model-Dependent Parameter Values

Parameter	Langmuir-Hinshelwood Model	95% Conf. Interval	CO Self-Exclusion Model	95% Conf. Interval
S_{CO}	3.53×10^{-6}	$(2.4\text{–}6.0) \times 10^{-6}$	7.6×10^{-5}	$(4.0\text{–}20.0) \times 10^{-5}$
k^o_{-1}	1.01×10^{7}	$(0.61\text{–}1.52) \times 10^{7}$	7.5×10^{15}	$(2.7\text{–}14.5) \times 10^{15}$
S_{O_2}	1.38×10^{-7}	$(0.85\text{–}2.2) \times 10^{-7}$	9.9×10^{-8}	$(7.0\text{–}14.0) \times 10^{-8}$
k^o_3	7.46×10^{9}	$(5.91\text{–}9.33) \times 10^{9}$	5.4×10^{10}	$(4.3\text{–}6.7) \times 10^{10}$
E_{-1}/R	6,950	(2,900–10,100)	13,900	(6,000–19,300)
E_3/R	5,150	(3,500–7,000)	5,800	(4,000–7,700)
N_{CO}	1.0	—	1.07	(1.06–1.08)*

*Based on low-conversion rate behavior, all other confidence intervals based on bifurcation point locations.

sion is very low, the oxygen consumption in the reactor will be negligibly different from that of the feed, i.e., $Y = Y_o = 1$. In addition, because of the low conversion, and the large amount of inerts in the feed, there will be a negligible change in the volumetric flow rate ($Q_n = 1$). Thus, in light of the above, combining Eqs. 13 and 14 yields:

$$1 - X = \frac{2F_{O_2}}{F_{CO}} K_2 \left(\frac{K_{-1}}{K_1 X}\right)^2 \tag{15}$$

Due to the dimensionalization that was used, K_1, K_{-1}, and K_2 depend on the flow rate and the feed composition. Since the issue to be resolved is the inability of the LH model to accurately predict the effect of flow rate on the value of F_{CO} at which a low to high conversion bifurcation occurs, it is necessary to explicitly relate X to F_{CO} and Q. Equation 15 becomes:

$$X^3 - X^2 + \frac{C_1}{F_{CO}^3 Q} = 0 \tag{16}$$

where C_1 is a constant defined in the Notation. In addition to Eq. 16, the bifurcation points must satisfy the condition that the derivative of F_{CO} with respect to X vanishes:

$$\frac{dF_{CO}}{dX} = (3X^2 - 2X)\left(\frac{F_{CO}^4 Q}{3C_1}\right) = 0 \tag{17}$$

Solving Eqs. 16 and 17 simultaneously gives $X = 2/3$ and,

$$F_{CO} = \left(\frac{27C_1}{4Q}\right)^{0.33} \tag{18}$$

Thus, the conversion of the simplified model at the bifurcation points is 33%, which compares favorably with the full model predictions of 35%. Furthermore, Eq. 18 leads to the bifurcation points varying as $Q^{-0.33}$, which matches exactly the predictions of the full LH model. For the values of the parameters specified in Table 1, the predicted locations of the bifurcation points from Eq. 18 are within 5% of the values determined by the full LH model. Equation 18 may also be used to predict the effect of temperature on the location of the low to high conversion bifurcation points. From Eq. 18 and the definition of C_1, it is seen that the value of F_{CO} at the bifurcation point will have an apparent activation energy of $0.67E_{-1}$. In the full LH model, a value of $E_{-1}/R = 6{,}950$ K was needed in order to describe the effect of temperature on the location of the low to high conversion bifurcation points. Thus, Eq. 18 predicts that the apparent activation energy of the low to high conversion bifurcation points should be 6,950 (2/3) or 4,633 K. This is in agreement with the experimental value of $E/R = 5{,}130$ K determined from Figure 4.

In addition to its inability to correctly predict the effect of flow rate on the bifurcation point locations, the LH model is also unable to correctly predict the reaction rates. This is shown in Figure 1, where predictions of conversion are presented. In the low-conversion region, it is seen that the predicted conversions are always much lower than the experimental observations. It is possible to choose model parameters that result in a closer match between the experimental and predicted conversions; however, in so doing the predicted bifurcation points no longer agree with the experimental values, and the predicted conversions on the high-conversion curve become significantly less than the experimentally observed value of 100%. In some cases the predicted region of multiplicity disappears when the kinetic parameters are adjusted to increase the conversion of the low rate branch.

For the LH model the reactor was assumed to be an isothermal CSTR with no inter- or intrapellet mass transfer limitations. The effects of these assumptions were examined individually to determine if any of the assumptions could be responsible for the mismatch between experimental data and model predictions, and it was concluded that the inability of the LH model to describe the experimental observations was not due to the experimental existence of nonisothermal behavior, imperfect mixing, or significant mass transfer limitations.

Attempts to describe the experimental data were made with a surface oxidation-reduction model (Sales et al., 1984) and a CO surface island formation model (Mukesh et al., 1984). Both of these models were able to quantitatively describe the bifurcation behavior presented in Figure 3, but neither model could accurately describe the effect of flow rate on the low to high conversion bifurcation points, Figure 5. Similarly to the LH model, both of these models predicted a $Q^{-0.33}$ variation of the location of the low to high conversion bifurcation points. These models also gave predictions of the low-conversion reaction rates that were much lower than the experimental observations. It is perhaps not surprising that these models were incapable of describing steady state data, since they were developed primarily to explain dynamic phenomena, such as self-sustained oscillations and dynamic response to step changes in feed flow rate, rather than to describe steady state behavior.

A modified CO surface island formation model was also examined. In this model the rate of oxygen adsorption was based on the island free area, rather than on the total area as in the previous surface island model. The predictions of the modified surface island model were significant improvements over the

LH model. The base case bifurcation behavior, the effect of temperature, and the effect of flow rate on the high to low conversion bifurcation curve were described as well by this model as by the LH model. This model could describe the effect of flow rate on the lower bifurcation points better than the LH model, the oxidation-reduction model, or the standard surface island model. The modified surface island model predicts that the lower bifurcation points will vary with $Q^{-0.5}$. This is midway between the experimental value of $Q^{-0.66}$ and the prediction of $Q^{-0.33}$ by the three previous models. The oxidation-reduction model, the standard surface island model, and the modified surface island model are examined in more detail in the supplementary material.

CO self-exclusion model

In the previous models it has been assumed that the number of sites available for O_2 adsorption is equal to that available for CO adsorption. This is not necessarily the case. Adsorption studies of oxygen on Pt (Wilson and Hall, 1970; Freel, 1972) indicate that saturation coverage of oxygen can vary between a fractional coverage of about 0.5 and 1.0. Herz and Marin (1980) have used a model that excludes oxygen from one half of the surface to describe the steady state oxidation of CO on supported platinum catalysts. Lynch (1984) used a similar oxygen self-exclusion model to describe CO oxidation during forced composition cycling. The main effect of oxygen self-exclusion is to maintain the CO conversion at close to 100% as CO concentration approaches zero. The oxygen self-exclusion model also eliminates the pathological steady state corresponding to complete oxygen surface coverage that otherwise occurs when the oxygen adsorption process is irreversible. However, simulations (Lynch, 1984) have shown that oxygen self-exclusion affects the bifurcation behavior negligibly. Thus, this phenomenon cannot be used to eliminate the discrepancies between the model predictions and the experimental observations.

Studies using CO, analogous to those using oxygen, have shown that a self-exclusion effect also occurs for CO adsorbed on platinum. Freel (1972), Dorling and Moss (1967), and Yao et al. (1979) have determined that for supported Pt with small average particle sizes (<5 nm), the maximum ratio of CO molecules adsorbed per Pt surface atom is 0.87 ± 0.07. In a mathematical model this effect can be described by requiring that an adsorbed CO molecule exclude other CO from an area equivalent in size to N_{CO} ($1 \le N_{CO} \le 1.25$) surface Pt atoms. In the classical LH model $N_{CO} = 1$. From the detailed derivation presented in the supplementary material, the net rate of CO adsorption will be given by:

$$R_1 = K_1 X(1 - \theta_{CO} - \theta_O)\frac{(1 - N_{CO}\theta_{CO})}{(1 - \theta_{CO})} - K_{-1}\theta_{CO} \quad (19)$$

In the CO self-exclusion model, Eqs. 19, 11, and 12 are used to describe the rates of steps 1 to 3. Using the parameters shown in Table 1, the CO self-exclusion model gave an excellent description of the steady state behavior of the CO oxidation reaction. Predictions of the effect of temperature and flow rate on the bifurcation behavior of the system match the experimental behavior exceedingly well. The superiority of the CO self-exclusion model over the LH model is most clearly seen by comparing Figure 5a with 5b. For the twelve bifurcation points in Figure 5b, the sum of the squares of the errors (SSE) is 4.37×10^{-7} when using the CO self-exclusion model. However, in Figure 5a, the SSE is 3.03×10^{-6} when using the LH model. This difference is statistically significant at the 0.7% level, which easily satisfies the 1% or 5% level normally used when testing hypotheses. For the other bifurcation points, the predictions of the two models are essentially equivalent. The improvement occurs because the CO self-exclusion model, unlike the LH model, is not restricted to a $Q^{-0.33}$ variation of the low to high conversion bifurcation points. A development similar to that presented in Eqs. 13 to 18 shows that the CO self-exclusion model predicts that the bifurcation points will vary with $Q^{-\gamma}$, where $0.33 < \gamma < 1.0$, depending on the value of N_{CO} (see the supplementary material for this analysis). The same analysis shows that the CO self-exclusion model can predict bifurcation point conversions between 33 and 100%. Using the parameters shown in Table 1, the CO self-exclusion model was able to match the experimentally observed value of $\gamma = 0.66$.

The CO self-exclusion model was also able to better describe the rate behavior for the low-conversion branch of the steady state rate curve, as shown in Figure 1. The SSE for the reaction rates is 3.9×10^{-3} from the CO self-exclusion model, compared to 4.9×10^{-1} for the LH model. This difference is statistically significant at the 0.02% level. The value of N_{CO} in Table 1 was arrived at by minimizing the SSE for the low-conversion rate behavior, with the constraint that the SSE for the bifurcation points also be a minimum. This procedure was used because it was found that the low-conversion rate behavior was particularly sensitive to the choice of N_{CO}. The estimation of all other parameters was based solely on minimizing the SSE for the bifurcation point locations.

The CO self-exclusion model is the only model examined herein that was able to quantitatively predict the bifurcation behavior as a function of flow rate. The CO self-exclusion model is also the only model that predicts conversions for the low conversion branch as high as those observed experimentally. For these reasons the CO self-exclusion model is the only kinetic model of those examined that can quantitatively describe all of the observed steady state multiplicity and rate behavior for CO oxidation on supported platinum.

The predictions shown in Figures 1 and 5b for the CO self-exclusion model were calculated by determining the steady state solution(s) of Eqs. 4 to 9 with the rates for steps 1 to 3 determined from Eqs. 19, 11, and 12. This calculation can be quite involved since the roots must be determined for a system of simultaneous nonlinear algebraic equations. However, this involved calculation is not always necessary because the reaction rate of the CO self-exclusion model can be expressed explicitly in terms of CO and O_2 concentrations by assuming that CO adsorption/desorption is at equilibrium, and oxygen surface coverage is at its steady state value. These two assumptions are implemented by setting Eqs. 19 and 8 equal to zero and solving for θ_{CO} and θ_O.

$$r_{CO_2} = k_3 L_m^2 \theta_{CO}\theta_O = \frac{2L_m^2 k_2 (k_3 k_1/k_{-1})^2 \epsilon^2 [CO]^2[O_2]}{\{2k_2[O_2] + k_3(k_1/k_{-1})\epsilon[CO] + k_3(k_1/k_{-1})^2\epsilon^2[CO]^2\}^2} \quad (20)$$

where

$$\epsilon = \left(\frac{1 - N_{CO}\theta_{CO}}{1 - \theta_{CO}}\right) = \frac{(C_2 - C_3) + \sqrt{(C_2 + C_3)^2 + 4C_2C_3C_4}}{2C_2(1 + C_4)} \quad (21)$$

$$C_2 = k_3(k_1/k_{-1})[CO]; \quad C_3 = 2k_2[O_2]; \quad C_4 = (N_{CO} - 1)(k_1/k_{-1})[CO] \quad (22)$$

For the particular values of rate constants listed in Table 1, the rate function becomes

$$r_{CO_2} = \frac{4.50 \times 10^{-14} T^{1.5} e^{(16,200/T)} \epsilon^2 [CO]^2[O_2]}{\left\{\begin{matrix}3.18 \times 10^3 \sqrt{T}[O_2] \\ + 1.88 \times 10^{-4} \sqrt{T} e^{(8,100/T)} \epsilon [CO] \\ + 6.54 \times 10^{-19} T e^{(22,000/T)} \epsilon^2 [CO]^2\end{matrix}\right\}^2} \quad (23)$$

where ϵ is determined using Eq. 21 with the values of C_2, C_3, and C_4 given in the Notation. When this rate expression is used in the design equation (component balance) for a CSTR,

$$Q_o([CO]_o - Q_n[CO]) - r_{CO_2} a_m = 0 \quad (24)$$

it is found that excellent quantitative predictions result for both the steady state rate behavior and the locations of the bifurcation points. The use of Eq. 20 is strongly recommended whenever it is desired to fit a rate function to steady state data for CO oxidation on platinum. In the fitting procedure, it is only necessary to estimate values for the quantities k_1/k_{-1}, k_2, k_3, and N_{CO}. A rate function of this form should also prove to be useful for describing steady state CO oxidation on many of the other noble metals.

Unfortunately, the results presented in this study do not provide the final word concerning the modeling of CO oxidation on platinum. This is because none of the models described in this study can quantitatively describe the complex reaction dynamics, such as chaos, self-sustained oscillations, and rate enhancement during forced composition cycling of the feed, that have often been observed during CO oxidation on supported platinum. Since of the models examined only the CO self-exclusion model can quantitatively describe the steady state behavior, it is this model that should be used as the basis for further development in any attempt to describe the various dynamic phenomena.

In further studies of this system, to be reported at a later date, it has been found that large increases in the time-average reaction rate occur when the feed composition is deliberately varied in a periodic fashion. This resonant behavior can be quantitatively described by using the CO self-exclusion model with the further modification that an adsorbate-induced surface phase change occurs. Since a model incorporating this effect has been shown to be capable of quantitatively describing self-sustained oscillatory behavior (Lynch et al., 1986), the preliminary results indicate that a single model will be able to provide a unified, consistent, description of the various steady state and dynamic phenomena for CO oxidation on platinum. This will be the focus of further studies of this system.

Conclusions

A systematic study of the effects of reactor temperature, feed composition, feed flow rate, and catalyst charge on multiplicity and rate behavior was conducted for the catalytic oxidation of carbon monoxide on Pt/Al_2O_3 in a recycle reactor. It was found that multiple steady states occur in a cusp-shaped region on a CO-O_2 feed composition diagram. Multiple steady states were found only when oxygen was in excess. As oxygen concentration or reactor temperature was increased, or as feed flow rate was decreased, the boundaries of the region of multiple steady states moved to higher carbon monoxide concentrations. An elementary step Langmuir-Hinshelwood mechanism was able to quantitatively describe the boundaries of the multiple steady state region for temperature variations. The LH mechanism could not quantitatively describe either the effect of feed flow rate on the multiplicity region boundary, or the absolute CO conversion of the low-conversion steady state.

Several other models were examined and gave results comparable to the LH model. These included a surface oxidation-reduction model, and a standard CO surface island formation model. A CO surface island model with a modified oxygen adsorption term gave better predictions than the LH model. The behavior predicted by this model was about midway between that of the LH model and the experimental observations. An elementary step Langmuir-Hinshelwood model for which CO is excluded from a small fraction of surface sites was the only model that was able to quantitatively predict all observed steady state phenomena.

Although the CO self-exclusion model can provide predictions of the steady state behavior for CO oxidation, it cannot quantitatively predict the very large time-average reaction rates observed during forced feed composition cycling. Further model development and experimental work is in progress to develop a complete understanding of all of the complex behavior observed for CO oxidation on platinum.

Acknowledgment

This work has been supported by the Natural Sciences and Engineering Research Council of Canada. Thanks are due to F. B. Russell for the use of computer programs for the homotopy-continuation method. W. R. C. Graham is grateful for a Province of Alberta Graduate Fellowship.

Notation

a_m = total surface area of supported catalyst; 3.17 m^2 for 4.95 g charge, 9.36 m^2 for 14.6 g charge, 27.8 m^2 for 43.6 g charge (based on Pt dispersion of 0.5)
C_1 = parameter, Eq. 16, $2F_{O_2}k_2a_mL_m^2(k_{-1}RT/k_1P)^2(PT_{ref}/P_{ref}T)$
C_2 = parameter, Eq. 22, $1.88 \times 10^{-4}\sqrt{T}e^{(8,100/T)}$[CO], $m^2/mol \cdot s$
C_3 = parameter, Eq. 22, $3.18 \times 10^3\sqrt{T}[O_2]$, $m^2/mol \cdot s$
C_4 = parameter, Eq. 22, $2.44 \times 10^{-16}\sqrt{T}e^{(13,900/T)}$[CO]
[CO] = reactor, and exit, CO concentration, mol/m^3
$[CO]_o$ = time-average feed CO concentration, $F_{CO}P/RT$, mol/m^3
$[CO_2]$ = reactor, and exit, CO_2 concentration, mol/m^3
E_{-1}/R = activation energy for CO desorption, K
E_3/R = activation energy for surface reaction, K
F_{CO} = time-average fraction CO in feed
F_{O_2} = time-average fraction O_2 in feed
k_1 = CO adsorption rate constant, $6.87\ S_{CO}\sqrt{T}/L_m$, $m^3/mol \cdot s$
k_{-1} = CO desorption rate constant, $k_{-1}^o \cdot \exp(-E_{-1}/RT)$, s^{-1}
k_{-1}^o = CO desorption preexponential factor, s^{-1}
k_2 = O_2 adsorption rate constant, $6.43\ S_{O_2}\sqrt{T}/L_m^2$, $m^3/mol^2 \cdot s$
k_3 = surface reaction rate constant, $k_3^o \cdot \exp(-E_3/RT)$, $m^2/mol \cdot s$

k_3^o = surface reaction preexponential factor, $m^2/mol \cdot s$
K_1 = dimensionless CO adsorption rate constant, $a_m L_m k_1/Q_o$
K_{-1} = dimensionless CO desorption rate constant, $a_m L_m k_{-1}/Q_o[CO]_o$
K_2 = dimensionless O_2 adsorption rate constant, $a_m L_m^2 k_2/Q_o$
K_3 = dimensionless surface reaction rate constant, $a_m L_m^2 k_3/Q_o[CO]_o$
L_m = adsorption capacity of the metal surface, 2×10^{-5} mol/m^2
N_{CO} = CO self-exclusion factor
$[O_2]$ = reactor, and exit, O_2 concentration, mol/m^3
$[O_2]_o$ = time-average feed O_2 concentration, $F_{O_2}P/RT$, mol/m^3
P = reactor pressure, 0.1 MPa absolute
P_{ref} = reference pressure, 0.101 MPa absolute
Q_n = ratio of exit to feed volumetric flow rates
Q = feed volumetric flow rate at standard conditions, m^3/s
Q_o = feed volumetric flow rate at reactor conditions, m^3/s
r_{CO_2} = rate of CO_2 formation, mol/m^2 Pt · s
R = gas constant, 8.314 m^3 · Pa/mol · K
R_1 = dimensionless rate of step 1
R_2 = dimensionless rate of step 2
R_3 = dimensionless rate of step 3
S_{CO} = CO sticking probability on catalyst
S_{O_2} = O_2 sticking probability on catalyst
t = time, s
T = reactor temperature, K
T_{ref} = reference temperature, 294 K
V = effective free volume of reactor, 2.1×10^{-4} m^3
X = dimensionless reactor CO concentration, $[CO]/[CO]_o$.
X_o = instantaneous dimensionless feed CO concentration (1 in this study)
Y = dimensionless reactor O_2 concentration, $[O_2]/[O_2]_o$
Y_o = instantaneous dimensionless feed O_2 concentration (1 in this study)
Z = dimensionless reactor CO_2 concentration, $[CO_2]/[CO]_o$
Z_o = instantaneous dimensionless feed CO_2 concentration (0 in this study)

Greek letters

α_m = ratio of bulk volume to metal surface capacitances, $[CO]_o V/a_m L_m$
ϵ = variable, Eq. 21, $(1 - N_{CO}\theta_{CO})/(1 - \theta_{CO})$
θ_{CO} = fractional CO surface coverage on the metal surface
θ_O = fractional oxygen surface coverage on the metal surface
τ = dimensionless time based on reactor residence time, $Q_o t/V$

Aluko, M., and H.-C. Chang, "Dynamic Modelling of a Heterogeneously Catalysed System with Stiff Hopf Bifurcations," *Chem. Eng. Sci.*, **41,** 317 (1986).

Beusch, H., P. Fieguth, and E. Wicke, "Thermisch und kinetisch verursachte Instabilitäten im Reaktionsverhalten einzelner Katalysatorkörner," *Chem. Ing. Tech.*, **44,** 445 (1972).

Chakrabarty, T., P. L. Silveston, and R. R. Hudgins, "Hysteresis Phenomena in CO Oxidation over Platinum-Alumina Catalyst," *Can. J. Chem. Eng.*, **62,** 651 (1984).

Conrad, F., and V. Treguer-Seguda, "Parameter Estimation in Some Diffusion and Reaction Models: An Application of Bifurcation Theory," *Chem. Eng. Sci.*, **39,** 705 (1984).

Cutlip, M. B., "Concentration Forcing of Catalytic Surface Rate Processes. I: Isothermal Carbon Monoxide Oxidation Over Supported Platinum," *AIChE J.*, **25,** 502 (1979).

Dorling, T. A., and R. L. Moss, "The Structure and Activity of Supported Metal Catalysts. II: Crystallite Size and CO Chemisorption on Platinum/Silica Catalyst," *J. Catal.*, **7,** 378 (1967).

Freel, J., "Chemisorption on Supported Platinum. II: Stoichiometry for Hydrogen, Oxygen, and Carbon Monoxide," *J. Catal.*, **25,** 149 (1972).

Goodman, M. G., M. B. Cutlip, C. N. Kenney, W. Morton, and D. Mukesh, "Transient Studies of Carbon Monoxide Oxidation Over Platinum Catalyst," *Surf. Sci.*, **120,** L453 (1982).

Graham, W. R. C., and D. T. Lynch, "Forced Composition Cycling During CO Oxidation on Platinum," Paper 132a, AIChE Ann. Meet., Chicago (Nov., 1985).

Gray, P., and S. K. Scott, "Autocatalytic Reactions in the Isothermal, Continuous Stirred-Tank Reactor: Isolas and Other Forms of Multistability," *Chem. Eng. Sci.*, **38,** 29 (1983).

Hegedus, L. L., S. H. Oh, and K. Baron, "Multiple Steady States in an Isothermal, Integral Reactor: The Catalytic Oxidation of Carbon Monoxide over Platinum-Alumina," *AIChE J.*, **23,** 632 (1977).

Heinemann, R. F., K. A. Overholser, and G. W. Reddien, "Multiplicity and Stability of Premixed Laminar Flames: An Application of Bifurcation Theory," *Chem. Eng. Sci.*, **34,** 833 (1979).

Herskowitz, H., and C. N. Kenney, "CO Oxidation on Pt Supported Catalysts. Kinetics and Multiple Steady States," *Can. J. Chem. Eng.*, **61,** 194 (1983).

Herz, R. K., and S. P. Marin, "Surface Chemistry Models of Carbon Monoxide on Supported Platinum Catalysts," *J. Catal.*, **65,** 281 (1980).

Kubicek, M., "Algorithm 502: Dependence of Solutions of Nonlinear Systems on a Parameter," *A.C.M. Trans. Math. Software*, **2,** 98 (1976).

Liljenroth, F. G., "Starting and Stability Phenomena of Ammonia-Oxidation and Similar Reactions," *Chem. Metall. Eng.*, **19,** 287 (1918).

Lynch, D. T., "On the Use of Adsorption/Desorption Models to Describe the Forced Periodic Operation of Catalytic Reactors," *Chem. Eng. Sci.*, **39,** 1325 (1984).

Lynch, D. T., and S. E. Wanke, "Oscillations during CO Oxidation over Supported Metal Catalysts. I: Influence of Catalyst History on Activity," *J. Catal.*, **88,** 333 (1984).

Lynch, D. T., G. Emig, and S. E. Wanke, "Oscillations during CO Oxidation over Supported Metal Catalysts. III: Mathematical Modeling of the Observed Phenomena," *J. Catal.*, **97,** 456 (1986).

Matsuura, T., and M. Kato, "Concentration Stability of the Isothermal Reactor," *Chem. Eng. Sci.*, **22,** 171 (1967).

Mukesh, D., W. Morton, C. N. Kenney, and M. B. Cutlip, "Island Models and the Catalytic Oxidation of Carbon Monoxide and Carbon Monoxide-Olefin Mixtures," *Surf. Sci.*, **138,** 237 (1984).

Oh, S. H., K. Baron, E. M. Sloan, and L. L. Hegedus, "Effects of Catalyst Particle Size on Multiple Steady States," *J. Catal.*, **59,** 272 (1979).

Sales, B. C., J. E. Turner, and M. B. Maple, "Oscillatory Oxidation of CO over Pt, Pd, and Ir Catalysts: Theory," *Surf. Sci.*, **114,** 381 (1982).

van Heerden, C., "Autothermic Processes: Properties and Reactor Design," *Ind. Eng. Chem.*, **45,** 1242 (1953).

Wilson, G. R., and W. K. Hall, "Studies of the Hydrogen Held by Solids. XVIII: Hydrogen and Oxygen Chemisorption on Alumina- and Zeolite-Supported Platinum," *J. Catal.*, **17,** 190 (1970).

Yao, H. C., M. Sieg, and H. K. Plummer, Jr., "Surface Interactions in the $Pt/\gamma\text{-}Al_2O_3$ System," *J. Catal.*, **59,** 365 (1979).

Manuscript received Apr. 22, 1986, and revision received Sept. 17, 1986.

See NAPS document no. 04456 for 14 pages of supplementary material. Order from NAPS c/o Microfiche Publications, P.O. Box 3513, Grand Central Station, New York, NY 10163. Remit in advance in U.S. funds only $7.75 for photcopies or $4.00 for microfiche. Outside the U.S. and Canada, add postage of $4.50 for the first 20 pages and $1.00 for each of 10 pages of material thereafter, $1.50 for microfiche postage.